ELSEVIER

Journal of Structural Geology 29 (2007) 1083–1098

JOURNAL OF STRUCTURAL GEOLOGY

www.elsevier.com/locate/jsg

High ductility of K-feldspar and development of granitic banded ultramylonite in the Ryoke metamorphic belt, SW Japan

Kazuhiko Ishii [a,*], Kyuichi Kanagawa [b], Norio Shigematsu [c], Takamoto Okudaira [d]

[a] *Department of Physical Science, Osaka Prefecture University, Gakuen-cho, Sakai 599-8531, Japan*
[b] *Department of Earth Sciences, Chiba University, Chiba 263-8522, Japan*
[c] *Geological Survey of Japan, National Institute of Advanced Industrial Science and Technology, Tsukuba 305-8567, Japan*
[d] *Department of Geosciences, Osaka City University, Osaka 558-8585, Japan*

Received 17 March 2006; received in revised form 18 January 2007; accepted 5 February 2007
Available online 1 March 2007

Abstract

Granitic mylonites from an upper greenschist facies mylonite zone in the Ryoke metamorphic belt, SW Japan show three types of microstructure with increasing mylonitization: (1) mylonite, (2) banded mylonite and (3) banded ultramylonite. The banded mylonites and ultramylonites include bands of quartz, biotite, K-feldspar, plagioclase > K-feldspar (>quartz + biotite) and K-feldspar > plagioclase > quartz. The inequality sign indicates abundance in modal proportion within a band. Microstructural and textural investigations by cathodoluminescence (CL), scanning electron microscopy (SEM) and electron back-scatter diffraction (EBSD) show that the microstructural changes from mylonites to banded ultramylonites have occurred through fracturing of plagioclase porphyroclasts, K-feldspar replacement by myrmekite, K-feldspar precipitation in fractures and tails and dislocation creep of quartz and K-feldspar. Development of the banded structure was promoted by high mobility via solution transfer of K-feldspar. Clear spatial distribution of constituent minerals in polyphase feldspar-rich bands, instead of homogeneous mixing of them, indicates that the grain boundary sliding was not the dominant deformation process.

Keywords: Granitic ultramylonite; Banded structure; Crystallographic preferred orientation (CPO); Microstructures of fine-grained aggregates

1. Introduction

Granitic mylonites and ultramylonites are major constituents in continental mid-crustal shear zones and commonly show compositional banding of fine-grained quartz bands and feldspar-rich bands containing porphyroclasts of feldspars (e.g. Behrmann and Mainprice, 1987). Within most ultramylonites, the banded structure is replaced by a homogeneous fine-grained mixture of quartz, feldspar, and other phases (e.g. Stünitz and Fitz Gerald, 1993; Fliervoet et al., 1997). These microstructures have been considered to indicate that important processes for strain softening, which brought localized shear zones, in mylonitic rocks include: (1) formation of continuous layers of a rheologically weak phase (Handy, 1990) and (2) a switch from dislocation creep to grain-size-sensitive creep resulting from grain-size reduction due to dynamic recrystallization, fracturing and/or phase transformation (Stünitz and Fitz Gerald, 1993; Fliervoet et al., 1997; Tsurumi et al., 2003).

In this paper, we describe the microstructural changes from mylonites to banded ultramaylonites in an upper greenschist facies mylonite zone in the Ryoke metamorphic belt, SW Japan. In these rocks, compositional banding is well developed even in ultramylonites. The microstructural analysis indicates that the development and persistence of the banded structure including nearly pure K-feldspar bands and polyphase feldspar-rich bands were achieved by high mobility of K-feldspar through myrmekite replacement, solution transfer and precipitation, and high deformability of K-feldspar by dislocation creep.

* Corresponding author. Tel.: +81 72 254 9729; fax: +81 72 254 9931.
E-mail address: ishii@p.s.osakafu-u.ac.jp (K. Ishii).

0191-8141/$ - see front matter © 2007 Elsevier Ltd. All rights reserved.
doi:10.1016/j.jsg.2007.02.008

2. Geological setting

The Cretaceous Ryoke metamorphic belt (e.g. Banno and Nakajima, 1992; Suzuki and Adachi, 1998; Fig. 1a) consists of abundant granitoids and an associated low-P/high-T metamorphic complex. The EW-trending Ryoke metamorphic belt is juxtaposed against the EW-trending high-P Sambagawa metamorphic belt at the Median Tectonic Line (MTL) in SW Japan. Ductile shear zones occur both along the southern margin of and within the metamorphic belt (e.g. Takagi, 1986; Imon et al., 2002).

In the Kishiwada district (Fig. 1b), foliated granitoids are widely distributed and strike EW with steep dips. They are divided into coarse-grained schistose hornblende-biotite tonalite (Chichionigawa tonalite), medium-grained schistose biotite granite (Konoyama granite), coarse-grained schistose hornblende-biotite granodiorite (Mizuma granodiorite), and fine- to coarse-grained schistose biotite granite (Jogo granite), from oldest to youngest according to their intrusive relations (Itihara et al., 1986). The Chichionigawa tonalite, Konoyama granite, and Mizuma granodiorite all contain abundant mafic inclusions such as hornblende diorite and biotite-hornblende quartz diorite. We recognized two strongly mylonitized zones with ENE-trend, slightly oblique to the boundaries among the schistose granitoids, whereas all the granitoids are more or less mylonitized. The southern shear zone is called the Kawai mylonite zone (Itihara et al., 1986; Takagi et al., 1988; Imon et al., 2002, 2004, Fig. 1b) and the other is the Konoyama mylonite zone (Takagi et al., 1988). The studied samples come from a western continuation of the Konoyama mylonite zone described by Takagi et al. (1988). The mylonitic foliation strikes EW to ENE and dips steeply toward north, and the stretching lineation is horizontal (Fig. 1c).

3. Analytical techniques

We documented the microstructures of these mylonitic rocks by means of optical, cathodoluminescence (CL) (Marshall, 1988), back-scattered electron (BSE) and orientation contrast (OC) (Lloyd, 1987; Prior et al., 1996) microscopy. In addition, crystallographic preferred orientations (CPO) of quartz and K-feldspar were measured by the SEM-based electron back-scatter diffraction (EBSD) technique (Randle, 2003). CL images were obtained by an optical microscope equipped with ELM-3R Luminoscope (Premier American Technologies: 12 kV, 0.7 mA, 7 mm ϕ beam; 60 s. Exp., ASA800) at Osaka City University. OC images and EBSD patterns were obtained using a JEOL JSM-6460 SEM at Chiba University with an accelerating voltage of 20 kV and a beam current of 4–6 nA (EBSD patterns) or 8–10 nA (OC images). Indexing of EBSD patterns and the misorientation analyses were done using the Channel 5 Software of HKL Technology. Chemical compositions of feldspar were analyzed using the Oxford EDS system (Link ISIS series L200I-S) attached to a JEOL JSM-840A SEM at Osaka Prefecture University using an accelerating voltage of 15 kV and beam current of 1.0 nA. Chemical compositions of biotite were analyzed using the EDAX EDS system (CDU LEAP detector and EDAX Genesis Spectrum software) attached to a JEOL JSM-5500 SEM at Osaka City University using an accelerating voltage of 15 kV and beam current of 0.5 nA. Corrections were made using the conventional ZAF method in both EDS system.

4. Microstructures

The protolith of studied mylonites is the Mizuma granodiorite. The Mizuma granodiorite is hornblende-biotite granodiorite containing large (1–3 cm) K-feldspar grains. Allanite, zircon, apatite and titanite are common accessory minerals. The Mizuma granodiorite is deformed more or less even outside the shear zones, indicated by the occurrence of dynamically crystallized quartz aggregates. The recrystallized grain sizes of quartz are variable among samples and even within a thin section ranging from several tens of micrometer to 1 mm. Deformational features of plagioclase such as fracturing along cleavage and bending of twin boundaries are common. K-feldspar is also fractured along cleavage and myrmekite is common around K-feldspar. Biotite shows bending and kinking of basal planes. In some samples, which include quartz bands, large lenticular (up to 3 mm in length) biotite grains have rims and tails of fine-grained biotite aggregates. These large biotite grains have Ti content of 0.25–0.42 for $O = 22$.

Studied mylonites are composed mainly of quartz (Qtz), plagioclase (Pl), K-feldspar (Kfs) and biotite (Bt) with minor chlorite, apatite, titanite, epidote, allanite, zircon and rutile. Some samples contain hornblende. Chlorite occurs mostly along fractures cutting the mylonitic foliation and likely originated from alteration after mylonitization. In these mylonites, the modal proportion of porphyroclasts decreases and compositional banding development increases from north to south. Based on these changes in microstructure, the mylonites are divided into type I, II and III, from north to south (Figs. 1c and 2), whereas the changes in microstructures between them are gradual. All microstructural and crystal fabric data are described for sections cut perpendicular to the foliation and parallel to lineation. These data are viewed downward and northward. All shear sense indicators, such as shape-preferred orientation of dynamically recrystallized quartz grains oblique to mylonitic foliation and asymmetric geometries of tails around porphyroclasts, indicate a sinistral sense of shear.

4.1. Type I

Type I mylonites consist of plagioclase and K-feldspar porphyroclasts, and quartz bands and biotite-rich bands forming planar layers or wrapping around the porphyroclasts (Fig. 2a and b).

The typical dimensions of recrystallized quartz grains in Qtz bands are 200–300 μm in length and 50–100 μm in width. Their size and shape are, however, variable depending on their position relative to porphyroclasts. Generally, in high-strain areas such as narrow zones between two porphyroclasts, recrystallized quartz grains have smaller grain size (<20 μm), a more elongated grain shape and straighter grain

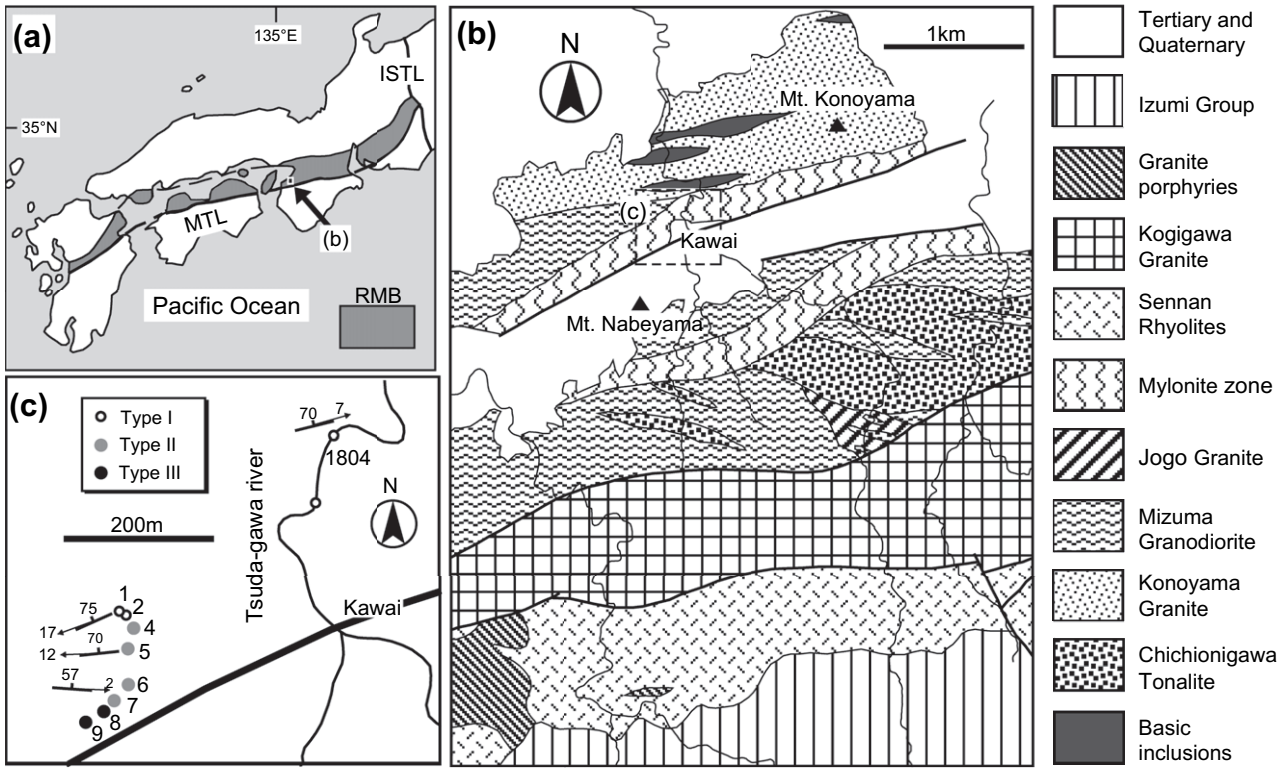

Fig. 1. (a) Index map of Ryoke metamorphic belt (RMB), SW Japan. MTL: Median Tectonic Line, ISTL: Itoigawa-Shizuoka Tectonic Line. (b) Geological map of Kishiwada district (modified after Itihara et al., 1986 using data in Takagi et al., 1988 and our unpublished data). (c) Distribution of different type of mylonitic rocks with sample numbers (1–9, 1804) and attitudes of mylonitic foliation and lineation.

boundaries than those in lower-strain areas. The recrystallized grains contain undulose extinction and subgrains. Most biotite grains in Bt-rich bands are 10–20 μm in width and 50–300 μm in length, but a few grains are larger than 300 μm in width and 1 mm in length. Biotite shows a wide range of Ti content (0.12–0.37 for O = 22). Bt-rich bands usually include titanite, apatite, plagioclase and/or quartz and their grain sizes are smaller than 100 μm.

The dominant deformational feature of plagioclase and K-feldspar porphyroclasts is fracturing along cleavage (Fig. 3). Some fractures are transgranular whereas others terminate within porphyroclasts. The minerals that fill the fractures are mostly quartz and otherwise chlorite, K-feldspar, calcite and epidote. The fracture-filling quartz is monocrystalline or aggregates with grain boundaries parallel to the opening directions of the fractures (Fig. 3a). These quartz grains show weak deformation features such as smooth undulose extinction. Microfractures without mineral-filling (expressed by offset of twin boundaries) and bending of twins are also common in plagioclase porphyroclasts. Myrmekite is common around K-feldspar porphyroclasts on the sides parallel to the mylonitic foliation (Fig. 3c–e). However, typical vermicular texture is limited to a narrow zone (<200 μm) adjacent to the K-feldspar porphyroclasts and the quartz grain-shape changes to globular further away from the contact. Some K-feldspar porphyroclasts have recrystallized along fractures and show undulose extinction (Fig. 3e). Tails composed of K-feldspar aggregates on K-feldspar and plagioclase porphyroclasts are also common and some of them include fragments of porphyroclasts (Fig. 3c–f). These fine-grained aggregates composed of K-feldspar, K-feldspar–plagioclase and plagioclase–quartz do not form continuous layers in type I mylonites (Fig. 2a). Fine-grained (20–100 μm) mono-mineralic plagioclase aggregates are also developed around plagioclase porphyroclasts but are less common.

Hornblende is deformed in a brittle manner. The hornblende clasts have tails composed of biotite, titanite and epidote. We could not find fine-grained elongate hornblende grains oriented parallel to the mylonitic foliation, so hornblende was likely to have been unstable during mylonitic deformation.

4.2. Type II

Type II mylonites are characterized by a banded structure consisting of alternating bands of fine-grained aggregates of different compositions (Fig. 2c and d). These include Qtz bands, Bt-rich bands, Kfs bands and Pl > Kfs (>Qtz + Bt) bands. The sign of inequality indicates abundance in modal proportion within a band. Therefore, type II mylonites are distinguished from type I mylonites by the development of Kfs bands and Pl > Kfs (>Qtz + Bt) bands. The modal proportions of biotite in Pl > Kfs (>Qtz + Bt) bands are variable, but are smaller than that of plagioclase in most bands.

Microstructures of Qtz bands and Bt-rich bands are the same as those in type I mylonites, but these bands are more

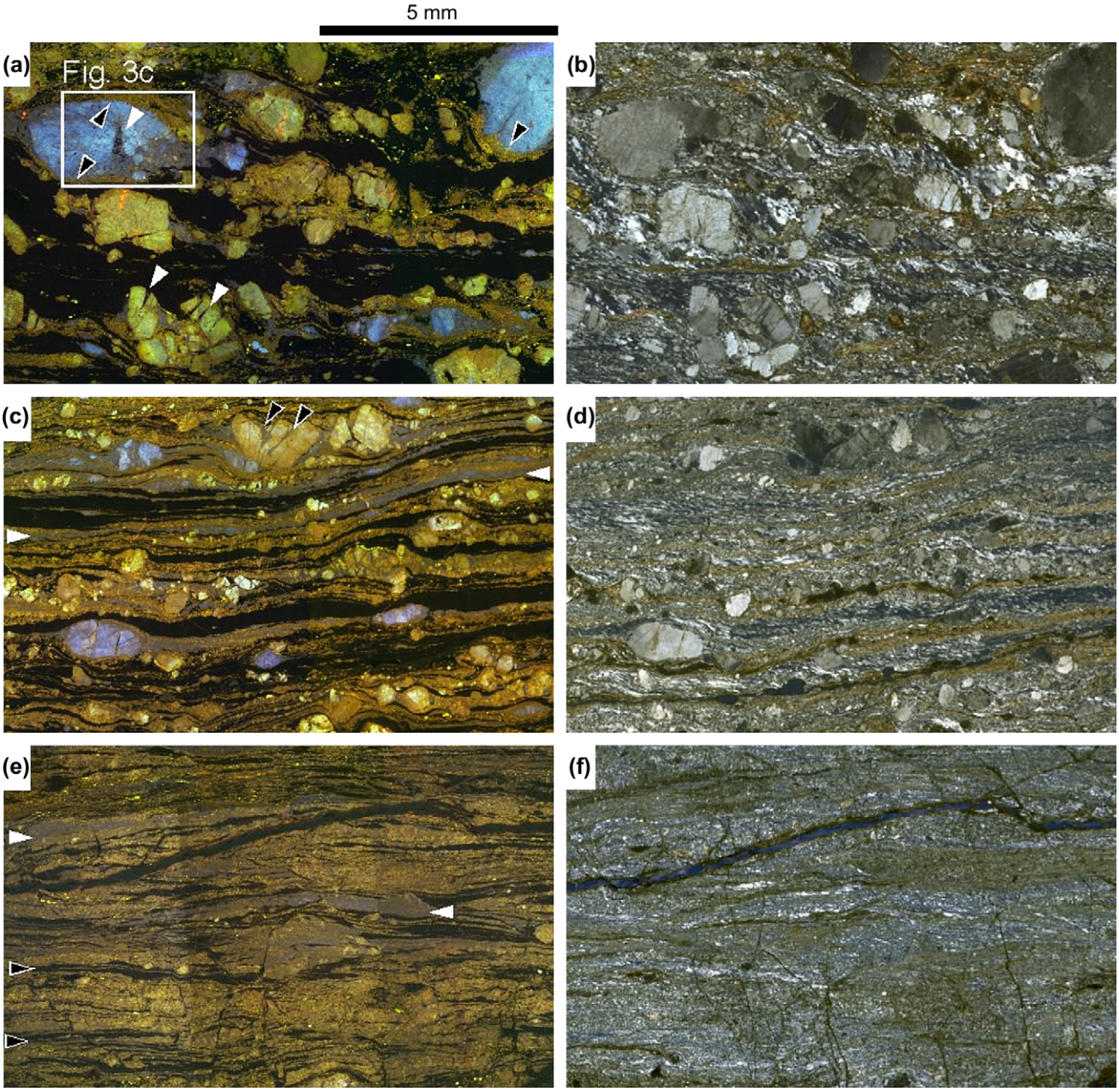

Fig. 2. CL images (a, c and e) and optical microphotographs (b, d and f) of mylonitic rocks. In CL images, K-feldspar shows blue color and plagioclase shows greenish yellow. Feldspar grains in matrix and tails show less bright color than porphyroclasts. Most of the black areas are composed of quartz and biotite. The optical microphotographs are taken by crossed polarized light with 45° oblique to the edges of images to avoid extinction of biotite. (a) and (b) Type I (sample 2). Qtz bands and Bt-rich bands form mylonitic foliation. Fractures of porphyroclasts are mostly filled with quartz (white arrows). Myrmekite around K-feldspar porphyroclasts is common (black arrows) and porphyroclasts have tails of Kfs or Kfs–Pl aggregates. (c) and (d) Type II (sample 7). The banded structure is composed of Kfs bands (white arrows), Pl > Kfs (>Qtz + Bt) bands, Qtz bands and Bt-rich bands. Fractures of porphyroclasts are mostly filled with K-feldspar (black arrows). (e) and (f) Type III (sample 8). The banded structure is composed of Kfs > Pl > Qtz bands (white arrows), Pl > Kfs (>Qtz + Bt) bands and Qtz bands (black arrow). The orientation of foliation and lineation and the shear sense are the same as Fig. 5.

planar than those in type I, reflecting larger magnitudes of finite strain and smaller contents and sizes of porphyroclasts (Fig. 2c and d). The typical dimensions of quartz grains in Qtz bands are 20–50 μm in width and 100–300 μm in length and their aspect ratios vary from 3 to more than 10 (Fig. 4a).

The microstructures of K-feldspar and plagioclase porphyroclasts are similar to those in type I, but gaps formed by fracturing of porphyroclasts are mostly filled with K-feldspar (Fig. 2c). K-feldspar in these fracture-fillings and in tails around porphyroclasts shows three types of microstructures: monocrystal, aggregates of elongate grains and aggregates of nearly equant grains. The long-axes of elongate grains are parallel to the mylonitic foliation or to the relative displacement direction of the fragments. The monocrystalline or aggregates of elongate grains developed in fracture-fillings and tails around plagioclase porphyroclasts (Fig. 4c and d). In contrast,

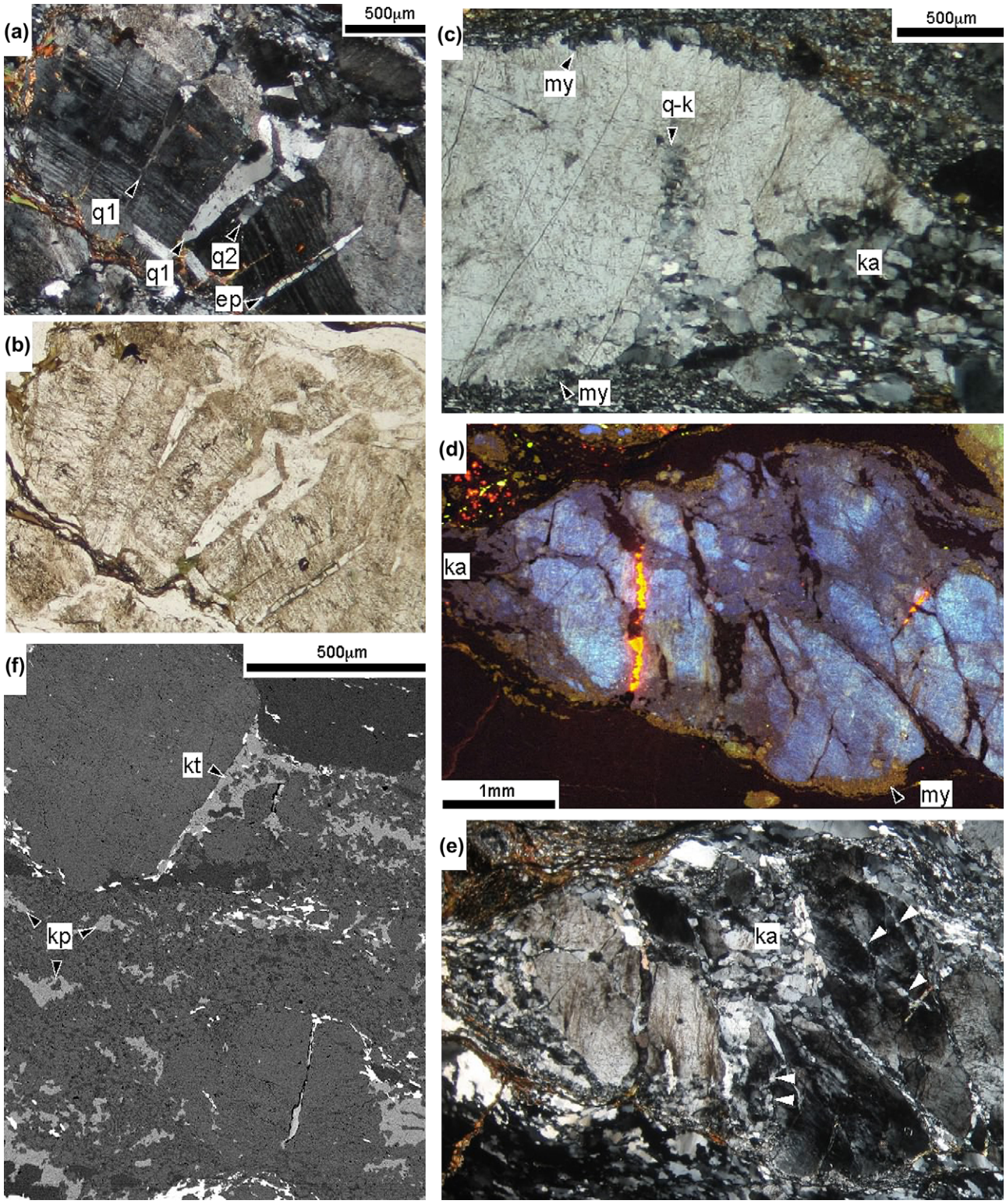

Fig. 3. Microstructures of type I mylonites (sample 2). (a) Optical microphotograph (CPL) of a plagioclase porphyroclast. Fractures are filled with monocrystalline quartz (q1), polycrystalline quartz (q2) and epidote (ep). The grain boundaries of the polycrystalline quartz are parallel to the opening direction of the fracture. (b) Optical microphotograph (PPL) of the same area of (a). (c) Optical microphotograph (CPL) of the area shown in Fig. 2a. A fracture in K-feldspar porphyroclast is filled with quartz and K-feldspar (q-k). Myrmekite (my) and tail of K-feldspar aggregate (ka) are developed around the porphyroclast. (d) CL image of a K-feldspar porphyroclast. Myrmekite (my) and tail of K-feldspar aggregate (ka) are developed around the porphyroclast. Fractures are mostly filled with quartz (black) and calcite (bright yellow). (e) Optical microphotograph (CPL) of the same area as (d). K-feldspar aggregate (ka) is also developed beside a fracture. (f) BSE image of fine-grained aggregates around porphyroclasts. Light gray: K-feldspar, medium gray: plagioclase, dark gray: quartz. K-feldspar tails (kt) on a plagioclase porphyroclasts include fragments of plagioclase. Most of Pl–Qtz aggregates are considered to be myrmekite around K-feldspar porphyroclasts or tails (kp). The orientation of foliation and lineation and the shear sense are the same as Fig. 5.

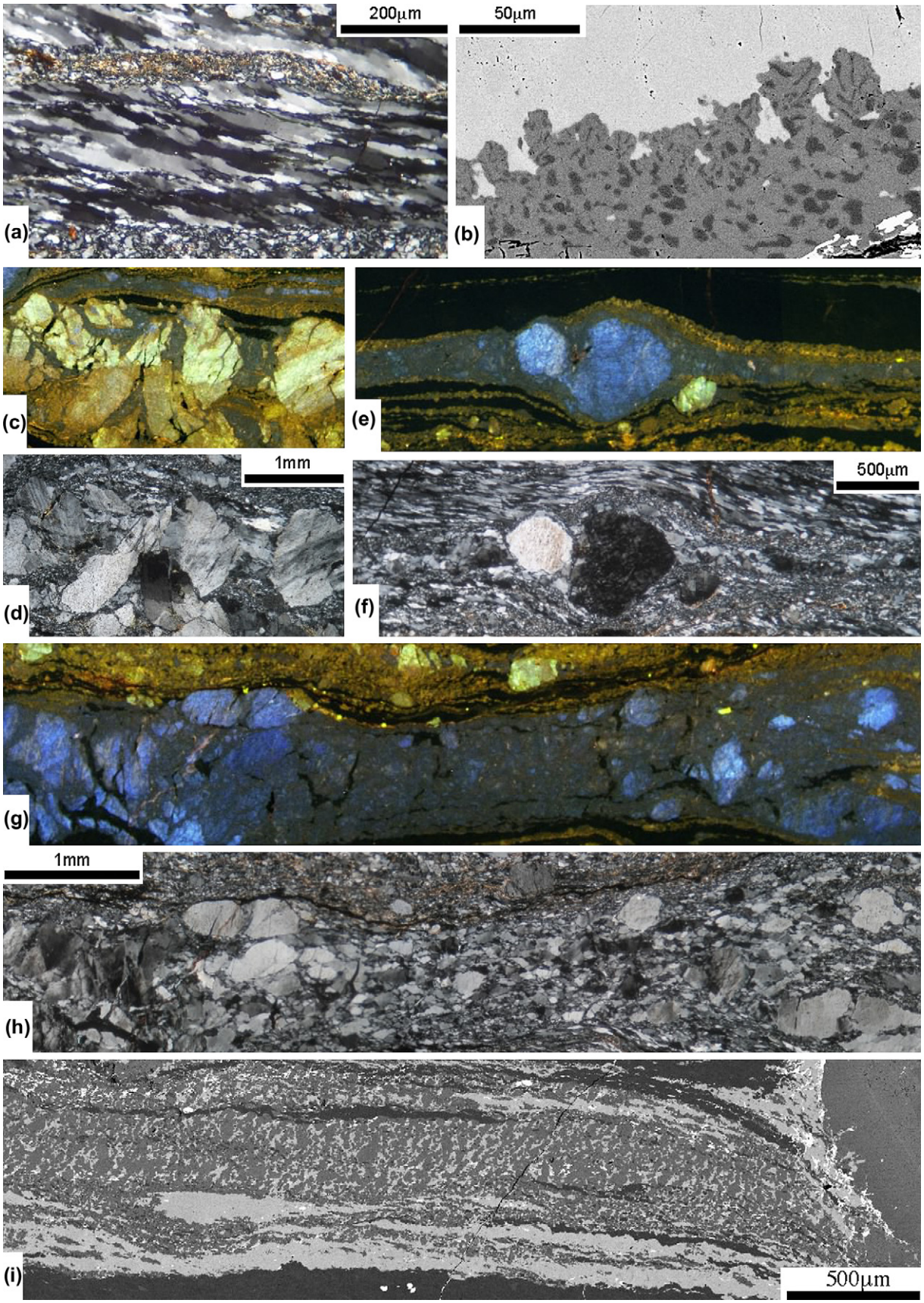

Fig. 4. Microstructures of type II mylonites (sample 7). (a) Optical microphotograph (CPL) of a Qtz band. (b) BSE image of a myrmekite that replaces the margin of a K-feldspar porphyroclast. Light gray: K-feldspar, medium gray: plagioclase, dark gray: quartz. (c) CL image of K-feldspar (dull blue) that fills gaps between

aggregates of nearly equant grains (100–300 μm) with undulose extinction are predominant as fracture-fillings and tails around K-feldspar porphyroclasts and these aggregates tend to form continuous Kfs bands (Fig. 4e–h). Myrmekite occurs around K-feldspar porphyroclasts (Fig. 4b) and even around tails composed of K-feldspar aggregates. The width of myrmekite with vermicular texture is narrower than that in type I (<50 μm).

The grain sizes of plagioclase in Pl > Kfs (>Qtz + Bt) bands are 20–100 μm. K-feldspar in Pl > Kfs (>Qtz + Bt) bands occurs interstitially between plagioclase grains. Both plagioclase and K-feldspar grains tend to be elongate at high angles to mylonitic foliation (Fig. 4i). Quartz, if present, is fine-grained (<20 μm) with globular shape and is mostly included in plagioclase. Biotite in Pl > Kfs (>Qtz + Bt) bands shows low Ti content (0.12–0.27 for O = 22).

4.3. Type III

Type III mylonites are banded ultramylonites characterized by alternating thin bands of fine-grained aggregates with a few small (<500 μm) plagioclase and rarely K-feldspar porphyroclasts (Fig. 2e and f). The microstructures of the fine-grained aggregate bands are similar to those in type II mylonites. However, Kfs > Pl > Qtz bands are present instead of Kfs bands and biotite is mostly included in Pl > Kfs (>Qtz + Bt) bands without forming Bt-rich bands. Microstructures of Qtz bands are quite homogeneous reflecting a very small content of porphyroclasts and are characterized by high ratio of grain boundaries to subgrain boundaries, recrystallized grain size (10–30 μm) similar to that of subgrains and nearly equant grain shapes (Fig. 5a).

Kfs > Pl > Qtz bands are characterized by K-feldspar aggregates with anastomosing thin layers of Pl > Qtz aggregate (Fig. 5b–d). Quartz grains are very fine-grained (<10 μm). These anastomosing layers align slightly oblique (10–20°) to the mylonitic foliation. The sense of obliquity is always antithetic with respect to the shear sense.

Fig. 6 shows the modal ratios of Pl, Kfs and Qtz in the different types of the fine-grained aggregates in type II and III mylonites. Qtz/(Pl + Qtz) values in Pl > Qtz aggregates (include myrmekite with vermicular quartz) are 0.18–0.28. Qtz/(Pl + Qtz) values in Kfs > Pl > Qtz bands are about 0.15, and those in Pl > Kfs (>Qtz + Bi) bands are equal or smaller than 0.15. Kfs > Pl > Qtz bands and Pl > Kfs (>Qtz + Bt) bands show clearly different Kfs/(Kfs + Pl) values. Therefore Kfs > Pl > Qtz bands and Pl > Kfs (>Qtz + Bt) bands are different in their modal ratios and spatial distributions (Fig. 5b). In addition, the K-feldspar in these bands shows different CPOs as described below.

4.4. Modal proportions

Modal proportions were determined by point counting on BSE and CL images (about 2000 points for a sample). Major constituent minerals and microstructural units (e.g. porphyroclasts, Qtz bands and Kfs > Pl > Qtz bands) of points for 5 samples were counted (Fig. 7). There is no large difference in bulk modal proportions of major constituent minerals among the samples, whereas the modal proportions of plagioclase and K-feldspar porphyroclasts decrease with increasing mylonitization (Fig. 7a). The modal proportion of Pl > Kfs (>Qtz + Bt) bands increase remarkably with increasing mylonitization, whereas the total modal proportion of Kfs aggregates, including tails on porphyroclasts, Kfs bands and Kfs > Pl > Qtz bands, are similar among the samples (Fig. 7b).

5. CPO

Fig. 8 shows CPOs of quartz grains in Qtz bands in type II and III mylonites. One <*a*> axis maximum is oriented slightly oblique to the lineation and the [*c*] axes are oriented normal to the lineation within the foliation plane (Y-maximum [*c*] axis fabric). Fig. 9 shows the result of a misorientation analysis on the same Qtz bands shown in Fig. 8. The misorientation angle distributions of neighbour point pairs show the highest peak at the lowest angle, and the frequency decreases gradually toward higher angle up to 30° (Fig. 9a and c). The maximum at 60° indicates a Dauphiné twin relationship because these pairs have misorientation axes parallel to the crystallographic [*c*] axis. The misorientation axes between neighbour point pairs with low misorientation angles are concentrated parallel to crystallographic [*c*] axis (Fig. 9b and d).

We used the crystallographic parameters of monoclinic orthoclase for the indexing of EBSD patterns of K-feldspar because the parameters of triclinic (maximum) microcline (Brown and Bailey, 1964) did not fit the EBSD patterns of K-feldspar in all kinds of studied fine-grained aggregates. Fig. 10 shows CPOs of K-feldspar grains in Pl > Kfs (>Qtz + Bt) bands in type II and III mylonites. These CPOs do not show strong concentrations. In contrast, K-feldspar grains in Kfs bands in type II mylonites (Fig. 11a and b) and Kfs > Pl > Qtz bands in type III mylonites (Fig. 11c) show rather strong CPOs. In these bands, the [010] axis (i.e. normal to (010) plane) orientations of K-feldspar grains are concentrated in the direction slightly oblique to lineation, and (100) (Fig. 11a) or (101) (Fig. 11b and (c) planes are subparallel to foliation. In addition, [001] (Fig. 11a) or $[\bar{1}01]$ (Fig. 11b and c) axes tend to orient normal to lineation within the foliation. The misorientation angle distribution of neighbour point pairs shows the highest peak at the lowest angle (Fig. 12a and c). Misorientation axes between neighbour point

plagioclase clasts (yellow). (d) Optical microphotograph (CPL) of the same area as (c). (e) CL image of a Kfs band (dull blue) extending from a K-feldspar porphyroclast (bright blue). (f) Optical microphotograph (CPL) of the same area as (e). (g) CL image of a Kfs band (dull blue) including K-feldspar porphyroclasts (bright blue). (h) Optical microphotograph (CPL) of the same area as (g). The K-feldspar porphyroclast on the left is highly deformed and fine-grained K-feldspar in the band show undulatory extinction. (i) BSE image of a Pl > Kfs (>Qtz + Bt) band. Light gray: K-feldspar, medium gray: plagioclase, dark gray: quartz. The orientation of foliation and lineation and the shear sense are the same as Fig. 5.

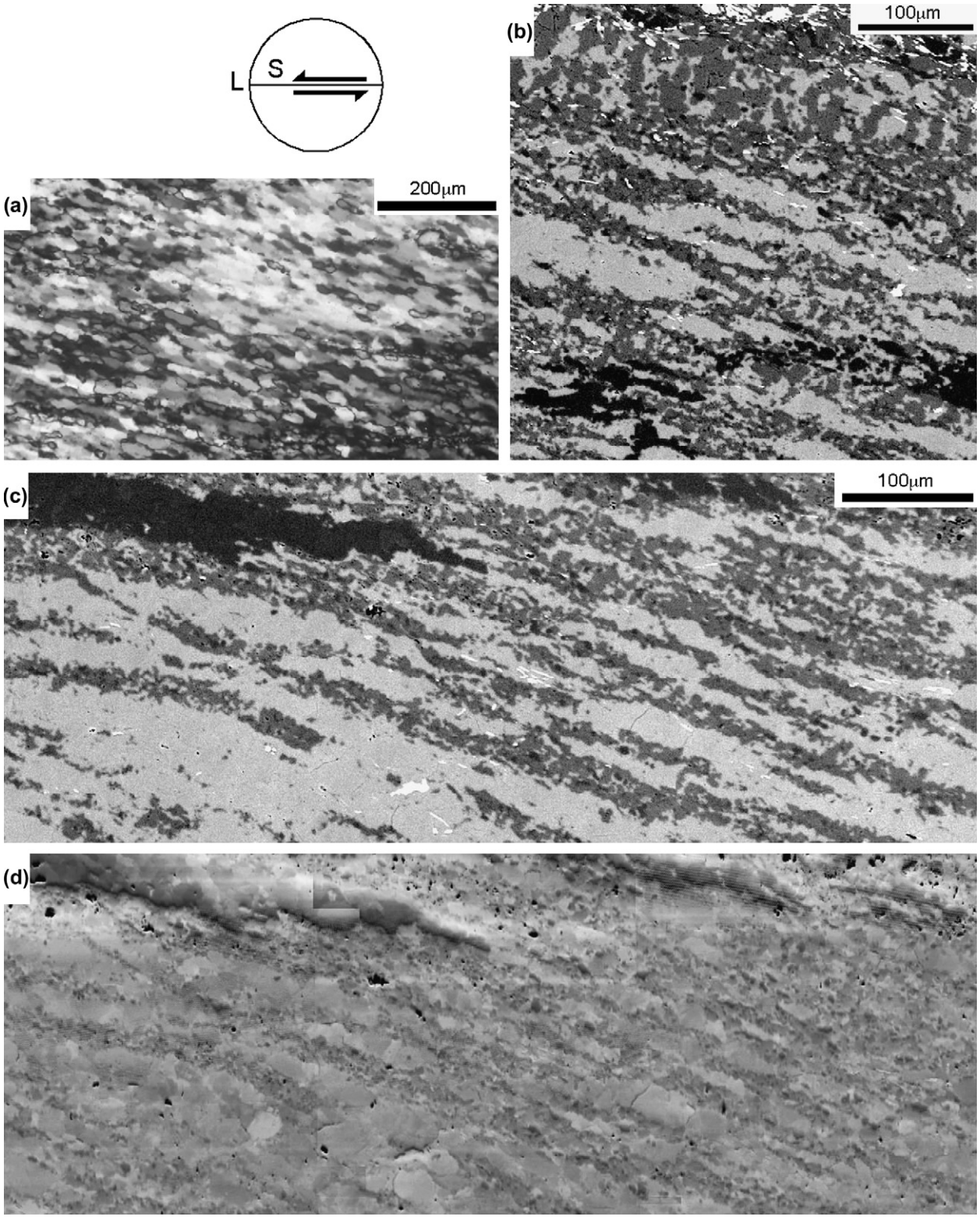

Fig. 5. Microstructures of type III mylonites (sample 8). (a) Optical microphotograph (CPL) of a Qtz band. (b) BSE image of a Pl > Kfs (>Qtz + Bt) band (top) and a Kfs > Pl > Qtz band (center to bottom) including a folded Qtz layer. Light gray: K-feldspar, medium gray: plagioclase, dark gray: quartz. (c) BSE image of a Kfs > Pl > Qtz band including Qtz layers (top). Light gray: K-feldspar, medium gray: plagioclase, dark gray: quartz. (d) OC image of the same area of (c). Lenses of K-feldspar are composed of fine-grained aggregate. The inset on the top left indicates the orientation of mylonitic foliation (S) and lineation (L) and the shear sense (coupled arrows).

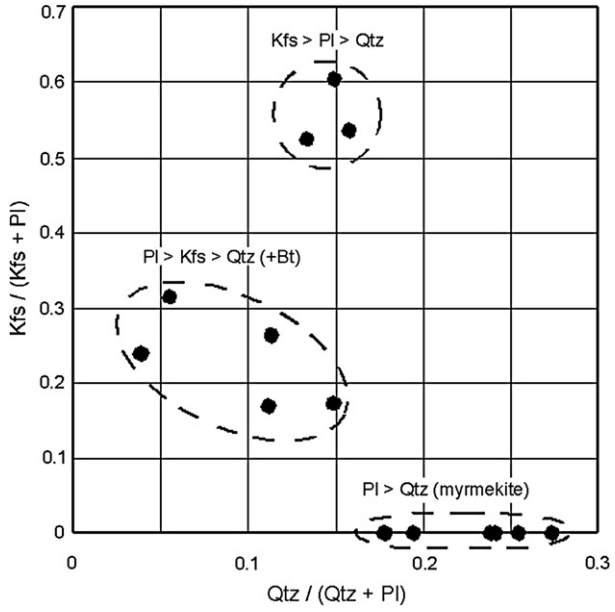

Fig. 6. Modal ratios among plagioclase, K-feldspar and quartz in fine-grained aggregates in type II and III mylonites.

pairs with low misorientation angles are concentrated parallel to crystallographic [001] or $[\bar{1}01]$ axes (Fig. 12b and d).

6. Chemical compositions of fine-grained feldspars

Plagioclase and K-feldspar in fine-grained aggregates (Pl > Kfs (>Qtz + Bt) bands, Kfs bands, Kfs > Pl > Qtz bands and Pl > Qtz aggregates) in type II and III mylonites show quite uniform composition. The composition of plagioclase is concentrated around An_{28-31} (Fig. 13). More albitic plagioclase (An_{10-15}, An_{22-25}) occurs irregularly within plagioclase with An_{28-31}. The composition of K-feldspar is concentrated around Or_{93-96} (Fig. 13).

7. Discussion

7.1. Deformation of Qtz bands

The CPO pattern with <*a*> axes subparallel to lineation and [*c*] axes normal to lineation within foliation (Fig. 8) suggests prism <*a*> slip system being dominant (e.g. Wilson, 1975; Bouchez, 1977; Lister and Dornsiepen, 1982). This inference is also supported by the orientations of misorientation axes between neighbour point pairs with low misorientation angles, which concentrate parallel to the crystallographic [*c*] axis (Fig. 9b and d), because in the case of slip due to edge dislocations producing subgrains separated by tilt boundaries, the misorientation axis between neighbour subgrain pairs should be perpendicular to both the slip plane normal and slip direction (e.g. Lloyd et al., 1997). Therefore, the Qtz bands have been deformed by dislocation creep with the dominant activity on the prism <*a*> slip system. The misorientation angles between neighbour point pairs show the highest frequency at low angles, with a gradual decrease with

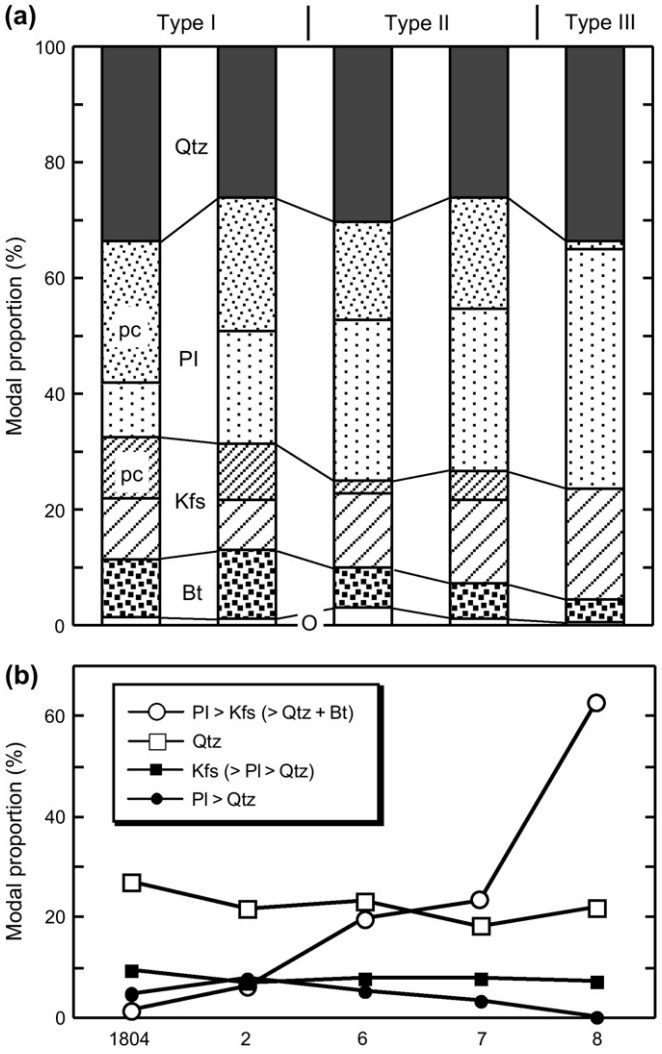

Fig. 7. Modal proportions of studied samples. (a) Bulk modal proportions of major constituent minerals. (b) Modal proportions of different type of fine-grained aggregates. Qtz: quartz, Pl: plagioclase, Kfs: K-feldspar, Bt: biotite, O: others, pc: porphyroclast.

increasing misorientation angle up to 30° (Fig. 9a and c). This trend indicates a continuous transition from low- to high-angle boundaries, suggesting progressive subgrain rotation as the dominant dynamic recrystallization process (Poirier and Nicolas, 1975; White, 1977; Guillope and Poirier, 1979; Neumann, 2000). In contrast, for the case of dislocation creep accommodated by grain boundary migration recrystallization (GBM of Stipp et al., 2002) or by both subgrain rotation and grain boundary migration (regime 3 of Hirth and Tullis, 1992; SGR/GBM transition of Stipp et al., 2002), misorientation angles are expected to show a frequency gap or minimum between low- and high-angle boundaries (Neumann, 2000; Wheeler et al., 2001, 2003). The measurement intervals of our misorientation analysis are at least several times smaller than average grain sizes and it is hard to expect the frequency gap or minimum between low- and high-angle boundaries by using a smaller measurement interval. In contrast, the smaller interval may result in the higher frequency of low-angle boundaries especially for Qtz bands in type III mylonites.

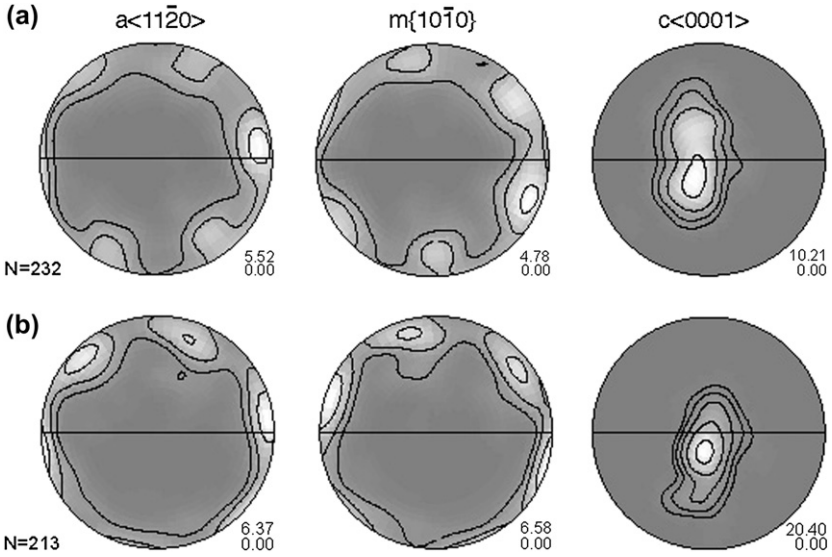

Fig. 8. CPOs of quartz in Qtz bands derived from manual EBSD measurements. (a) Type II (sample 7). (b) Type III (sample 8). Equal-area lower hemisphere projection using David Mainprice's software (PF2 k). The orientation of foliation and lineation and the shear sense are the same as Fig. 5. *N* is number of points measured. Contour lines are 1, 2, 4, 8 and 16 multiples of uniform distribution. Maximum and minimum densities are indicated on the lower right. Darker shadings indicate lower distribution densities.

Elongated recrystallized grains with subgrains (Fig. 4a) and the recrystallized grain size similar to that of subgrains (Fig. 5a) also indicate that Qtz bands have been deformed by climb-accommodated dislocation creep accompanied by rotation recrystallization (regime 2 of Hirth and Tullis, 1992; SGR of Stipp et al., 2002). However, optical microstructures are variable even in a thin section especially depending on the position relative to porphyroclasts. In the strain shadow (low strain) areas, quartz aggregates show a larger grain size, less elongated grain shapes and more curved or irregular grain boundaries than high-strain areas, indicating a greater activity of grain boundary migration due to a lower strain rate.

For quartz aggregates, slip in the <*a*> direction dominates at low to middle metamorphic grade conditions whereas [*c*] slip dominates in higher metamorphic grades. The transition of the slip direction from <*a*> to [*c*] has been considered to occur at 550–600 °C or higher temperatures (e.g. Lister and Dornsiepen, 1982; Blumenfeld et al., 1986; Mainprice et al., 1986; Okudaira et al., 1995). Slip in the <*a*> direction occurs predominantly on basal, rhombohedral and prism planes, and the prism <*a*> slip system becomes activated at higher temperature than basal <*a*> and rhomb <*a*> slip systems (e.g. Takeshita and Wenk, 1988). This transition of dominant slip system from basal <*a*> and rhomb <*a*> to prism <*a*> has been considered to occur at middle to upper greenschist facies conditions, which correspond to temperatures of 400–500 °C (Wilson, 1975; Schmid and Casey, 1986; Mancktelow, 1987; Sakakibara, 1995; Stipp et al., 2002). However, magnitude of strain and proportion of recrystallization can also affect the transition (Heilbonner and Tullis, 2002).

The dynamic recrystallization mechanism of quartz also varies according to deformation conditions. Grain boundary migration dominates over subgrain rotation at higher temperatures, lower strain rates, higher 'water' contents and thus lower flow stresses (Hirth and Tullis, 1992; Stipp et al., 2002, 2006). The transition from subgrain rotation to grain boundary migration corresponds to the transition of dominant slip system from basal <*a*> and rhomb <*a*> to prism <*a*> in several areas (Schmid and Casey, 1986; Mancktelow, 1987; Shigematsu and Yamagishi, 2002; Stipp et al., 2002). However, some exceptions have been also reported (Hippertt, 1998; Tagami and Takeshita, 1998; Yagi and Takeshita, 2002).

The microstructures of quartz aggregates in our samples described above are consistent with upper greenschist facies deformation conditions (400–500 °C) using criteria mentioned above. This conclusion is supported by the mineral compositions of the mylonites and chemical compositions of feldspars in fine-grained aggregates (Fig. 13).

7.2. Development of Pl > Kfs (>Qtz + Bt) bands

Pl > Kfs (>Qtz + Bt) bands are characterized by fine-grained plagioclase and interstitial K-feldspar that tends to align at high angle to the bands (Figs. 4i and 5b). These microstructures indicate that K-feldspar have been precipitated from solution to fill spaces between plagioclase fragments. Quartz in Pl > Kfs (>Qtz + Bt) bands is very fine-grained and is included in plagioclase. In addition, the modal ratios of quartz and plagioclase are the same as or smaller than those in Pl > Qtz aggregates (Fig. 6). Therefore, Pl > Kfs (>Qtz + Bt) bands likely have developed through fracturing (separation) along cleavage planes of plagioclase porphyroclasts and along grain boundaries within Pl > Qz aggregates, and filling the space by K-feldspar. Pl > Kfs (>Qtz + Bt) bands with high biotite content may have developed through filling the space along the grain boundaries of Bt-rich bands (mostly Bt-Pl aggregates) by K-feldspar or filling the space between the clasts of plagioclase by K-feldspar and biotite.

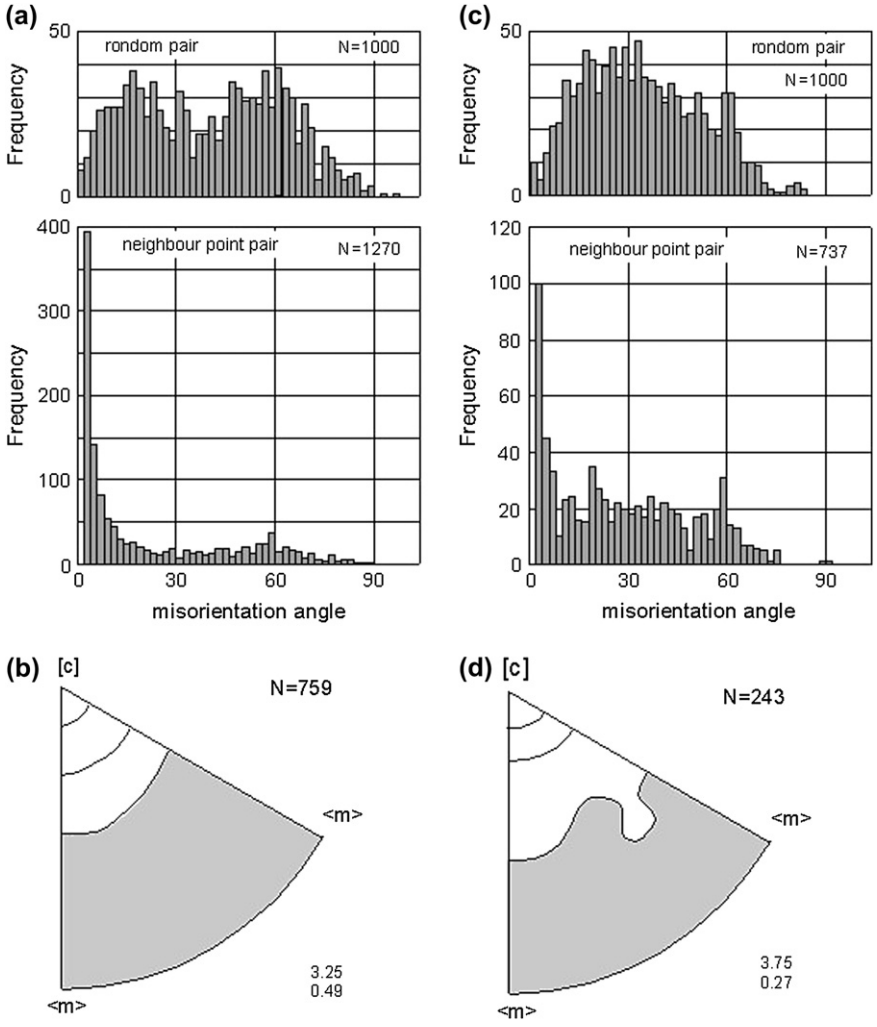

Fig. 9. Misorientation analysis of neighbour point pairs for Qtz bands. (a) and (b) The same Qtz band as Fig. 8a. 40×40 points with 5 μm spacing (i.e. 200 μm × 200 μm area) are analyzed. (c) and (d) The same Qtz band as Fig. 8b. 50×20 points with 4 μm spacing (i.e. 200 μm × 80 μm area) are analyzed. (a) and (c) Random pair and neighbour point pair misorientation angle distribution. Misorientation angles of neighbour point pairs lower than 2° are excluded. (b) and (d) Inverse pole figure showing misorientation axis distribution for misorientation angles that range 2–15°. Equal-area upper hemisphere projection. Contour lines are 1, 2, and 3 multiples of uniform distribution and the gray area indicates distribution density lower than the uniform. Maximum and minimum densities are indicated on the lower right. *N* is number of pairs.

Similar microstructures of fine-grained bands composed of Pl + Kfs ± Qtz ± mica in mylonites have been described by Behrmann and Mainprice (1987), Fliervoet et al. (1997), Tsurumi et al. (2003) and Ree et al. (2005). In contrast, the ultramylonites described by Fliervoet et al. (1997) and Tsurumi et al. (2003) show a homogeneous mixture of all phases, indicating that all components became mixed during further deformation by grain boundary sliding. However, in our ultramylonites Pl > Kfs (>Qtz + Bt) bands rarely show homogeneous mixing. Therefore, it seems unlikely that grain boundary sliding has been the dominant deformation process.

7.3. Development of Kfs bands and Kfs > Pl > Qtz bands

Kfs bands are composed of nearly equant fine-grained K-feldspar showing undulose extinction (Fig. 4e–h), and have CPOs (Fig. 11a and b). These suggest a deformation by dislocation creep. CPOs (Fig. 11a and b) and misorientation-axes orientations between neighbour point pairs with low misorientation angles (Fig. 12b and d) may suggest dominant activity of (100)[010] or (101)[010] slip system. The activity of (100)[010] slip system may also account for the CPO developed in a banded mylonite (stage III) of Schulmann et al. (1996), as optical directions γ (parallel to [010] axis) are oriented almost normal to the single girdle of quartz *c*-axis fabric. However the Burgers vector [010] is long ($b = 0.13$ nm), and a large Peierls stress is expected for this Burgers vector, i.e. the dislocations with this Burgers vector are hard to slip (e.g. Tullis, 1983). To confirm the dominant slip systems, detailed TEM analyses are needed. High ductility of K-feldspar in greenschist facies condition has not been reported except for elongate aggregates of K-feldspar in granitic mylonites from the Hatagawa Shear Zone, Japan (Tsurumi et al., 2003).

Quartz that fills the fractures in plagioclase and K-feldspar porphyroclasts (Fig. 3) and K-feldspar that fills fractures in plagioclase porphyroclasts (Fig. 4c and d), showing

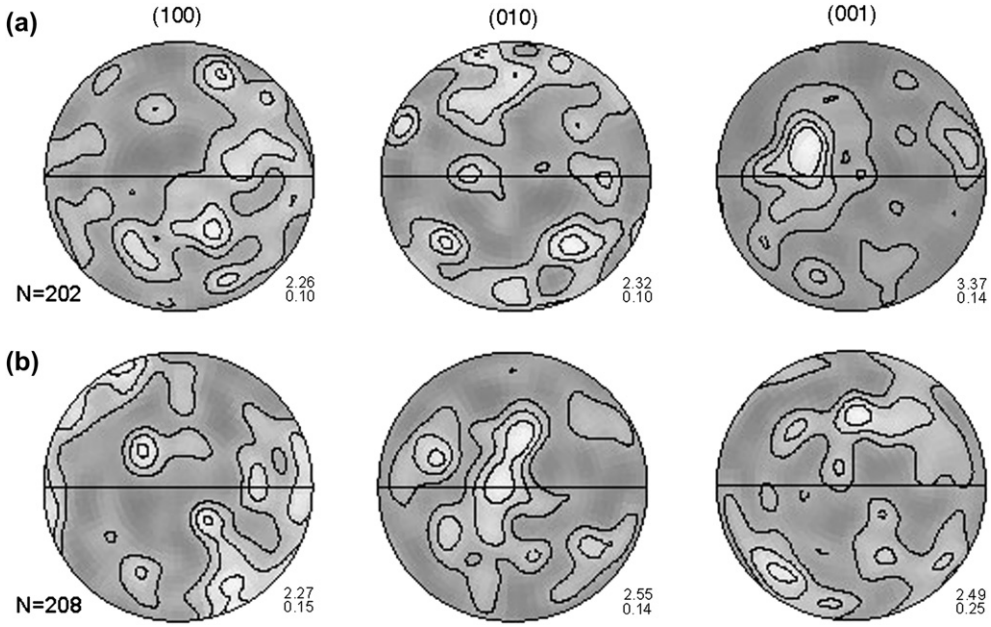

Fig. 10. CPOs of K-feldspar in Pl > Kfs (>Qtz + Bt) bands derived from manual EBSD measurements. (a) Type II (sample 7, the band shown in Fig. 4i). (b) Type III (Sample 8). Contour lines are 1, 1.5, 2 and 2.5 multiples of uniform distribution. The others are the same as Fig. 8.

microstructures of monocrystalline or aggregates with grain boundaries parallel to the opening direction, are considered to have been precipitated from solution. In contrast, there are two possible origins for fine-grained K-feldspar along fractures in K-feldspar porphyroclasts (Fig. 3c–e): precipitation from solution and dynamic recrystallization along fractures. The same relation applies to K-feldspar tails on K-feldspar porphyroclasts (Fig. 3c–e). Considering the large activity of solution transfer and precipitation of K-feldspar indicated by the development of Pl > Kfs (>Qts + Bt) bands, the precipitation from solution may be the dominant process for the development of Kfs bands, and then they deformed by dislocation creep. Some K-feldspar porphyroclasts are highly deformed (Fig. 4g and h) and others are less deformed (Fig. 4e and f). This difference may be due to the crystallographic orientation of K-feldspar porphyroclasts. Relative importance between the dislocation creep and the precipitation from solution for the development of Kfs bands may vary among bands.

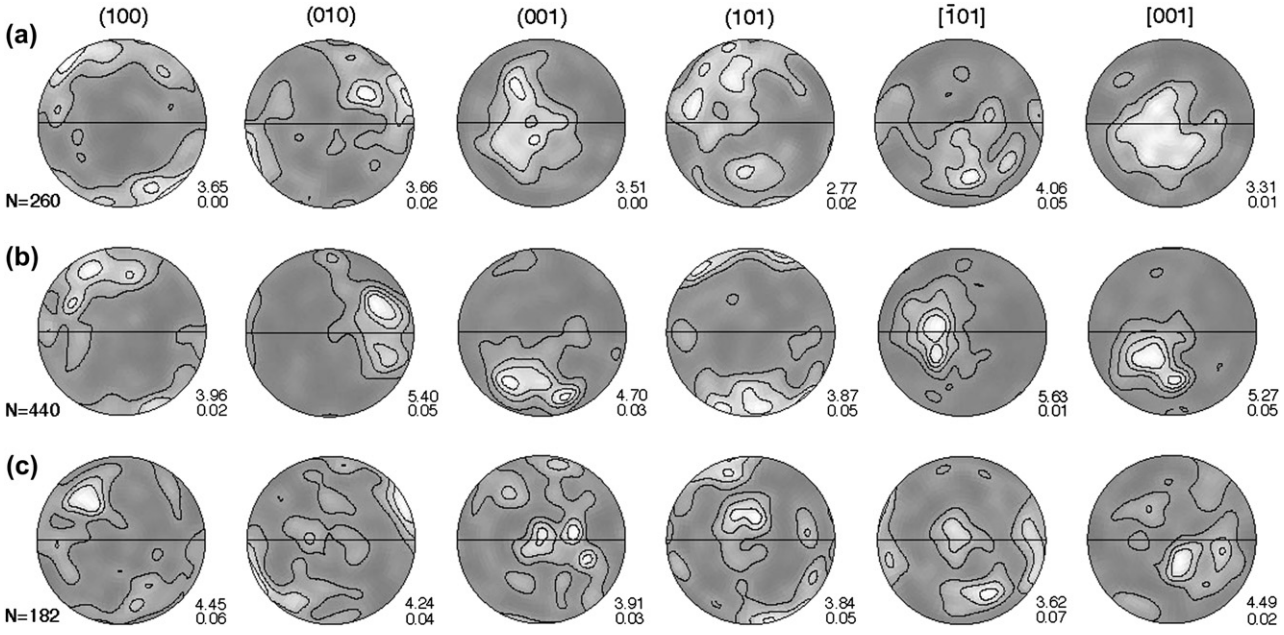

Fig. 11. CPOs of K-feldspar in Kfs bands and a Kfs > Pl > Qtz band derived from manual EBSD measurements. (a) Kfs band shown in Fig. 4g (Type II, sample 7). (b) Kfs band shown in Fig. 4e (Type II, sample 7). (c) Kfs > Pl > Qtz band shown in Fig. 5c (Type III, sample 8). Contour lines are 1, 2, 3 and 4 multiples of uniform distribution. The others are the same as Fig. 8.

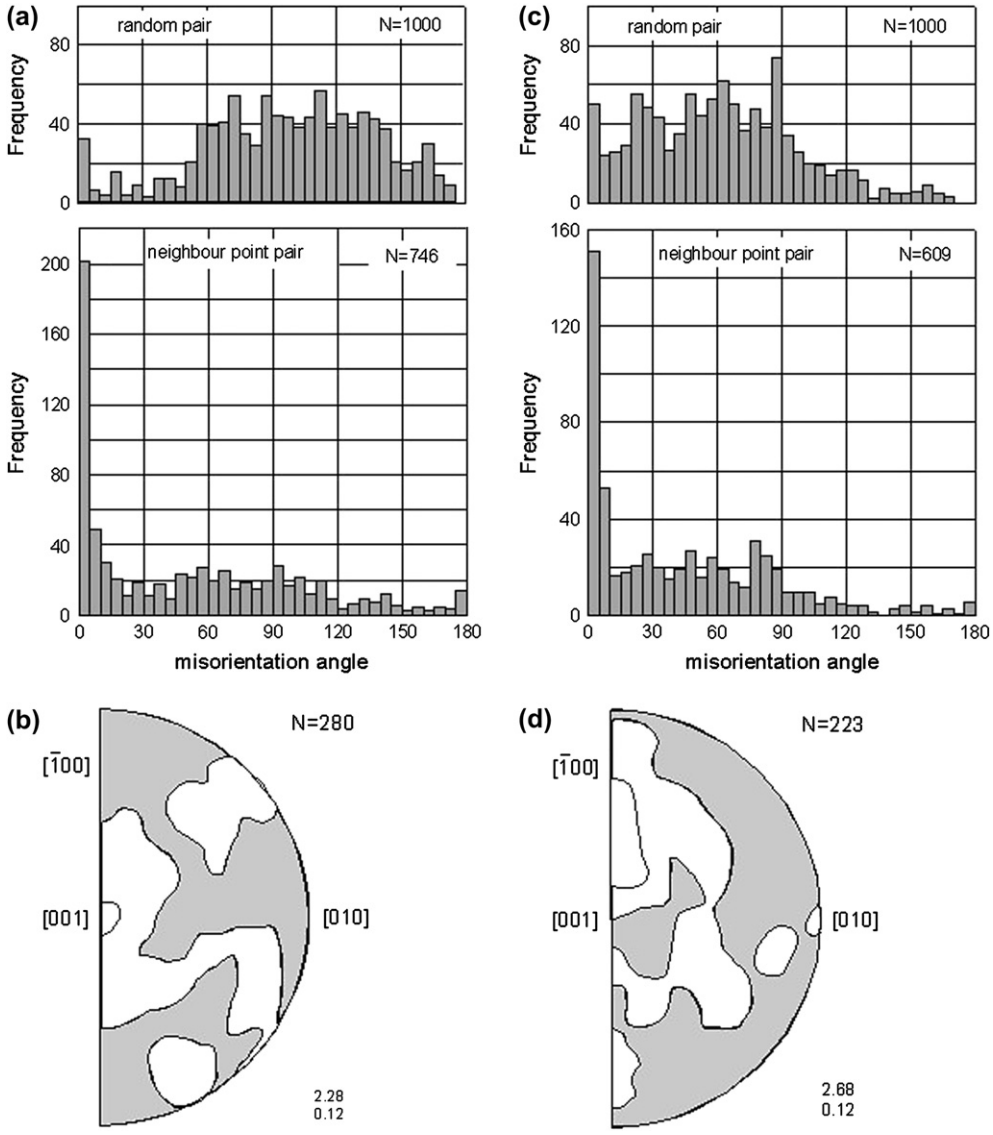

Fig. 12. Misorientation analysis of neighbour point pairs for Kfs bands in type II mylonites (sample 7). (a) and (b) The same Kfs band as Fig. 11a. 40 × 25 points with 10 μm spacing (i.e. 400 μm × 250 μm area) are analyzed. (c) and (d) The same Kfs band as Fig. 11b. 50 × 20 points with 8 μm spacing (i.e. 400 μm × 160 μm area) are analyzed. (a) and (c) Random pair and neighbour point pair misorientation angle distribution. Misorientation angles of neighbour point pairs lower than 2° are excluded. (b) and (d) Inverse pole figure showing misorientation axis distribution for misorientation angles that range 2–15°. Contour lines are 1 and 2 multiples of uniform distribution. The others are the same as Fig. 9.

Kfs > Pl > Qtz bands developed in type III ultramylonites are characterized by uniform and oblique orientation of thin anastomosing layers of Pl > Qtz aggregates. This microstructure is consistent with the typical orientation of myrmekite in mylonites that is approximately normal to maximum shortening direction (e.g. Simpson and Wintch, 1989; Menegon et al., 2006). Modal composition (Fig. 6) and small grain size of quartz (Fig. 5b and c) also indicate that these Pl > Qtz aggregates were originated from myrmekite. In addition K-feldspar in a Kfs > Pl > Qtz band show CPO (Fig. 11c). Therefore, Kfs > Pl > Qtz bands are considered to have developed through dislocation creep of Kfs bands and simultaneous formation of myrmekite along grain boundaries of K-feldspar. Grain boundary diffusion may contribute to the deformation because the formation of myrmekites (Pl > Qtz aggregates) within Kfs bands needs transportation of elements along grain boundaries.

7.4. Grain-size reduction and development of banding

The microstructural changes in the studied mylonites include a decrease in modal proportion and grain size of plagioclase and K-feldspar porphyroclasts, a development of Pl > Kfs (>Qtz + Bt) bands and Kfs bands and an increase in modal proportion of Pl > Kfs (>Qtz + Bt) bands (Figs. 2 and 7). Type II mylonites are distinguished from type I mylonites by the development of Pl > Kfs (>Qtz + Bt) bands and Kfs bands, and the change in the dominant fracture-filling mineral from quartz to K-feldspar. These features, together with interstitial K-feldspar within Pl > Kfs (>Qtz + Bt) bands,

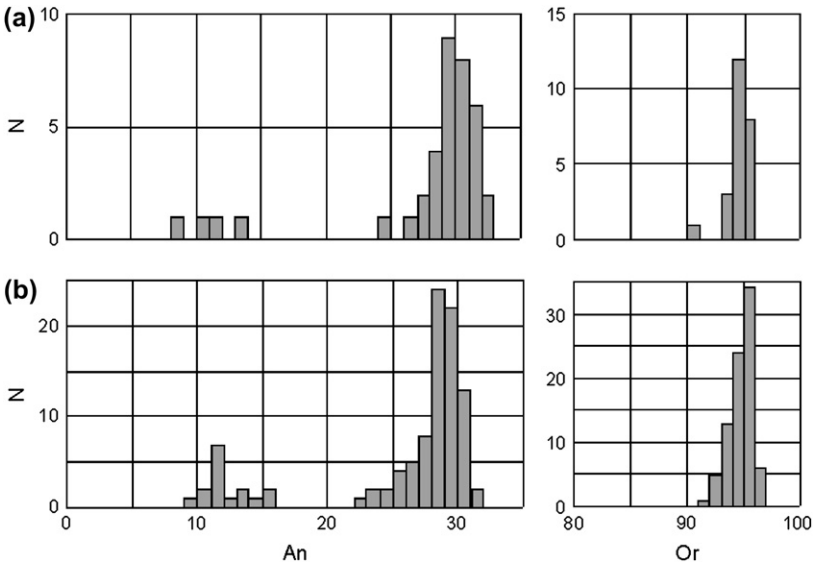

Fig. 13. Anorthite components of plagioclase (An) and Orthoclase components of K-feldspar (Or) in fine-grained aggregates. (a) Type II (sample 7). (b) Type III (sample 8).

indicate that high mobility of K-feldspar by solution transfer promotes the development of banding.

In the studied samples, porphyroclasts of plagioclase and K-feldspar were deformed dominantly by fracturing along cleavage. Myrmekite-forming reaction was also an important process for the grain-size reduction of K-feldspar porphyroclasts. K-feldspar replacement by myrmekite can be expressed as

$$\text{K-feldspar} + \text{Na}^+ + \text{Ca}^+ = \text{plagioclase} + \text{quartz} + \text{K}^+ \qquad (1)$$

Since there is no large differences in the modal proportions of K-feldspar among the samples (Fig. 7a), the aqueous K^+ is considered to have precipitated as K-feldspar in fractures, tails on porphyroclasts, Pl > Kfs (>Qtz + Bt) bands and Kfs bands (cf. Simpson and Wintch, 1989). K-feldspar in tails and Kfs bands was further replaced by myrmekite. Simultaneously, myrmekite (mostly Pl > Qtz aggregates with globular quartz) itself changed into Pl > Kfs (>Qtz + Bt) bands by the precipitation of K-feldspar in the space along grain boundaries. In this way, the modal proportion of porphyroclasts decreased to zero and that of Pl > Kfs (>Qtz + Bt) bands increased up to more than 60% with increasing mylonitization.

Type III ultramylonites are characterized by the banded structure composed of Qtz bands, Pl > Kfs (>Qtz + Bt) bands and Kfs > Pl > Qtz bands, instead of a homogeneously mixed polyphase matrix (cf. Stünitz and Fitz Gerald, 1993; Fliervoet et al., 1997). The development and persistence of the banded structure without boudinage during deformation suggest these feldspar-rich bands were as ductile as Qtz bands. The high mobility of K-feldspar through myrmekite replacement, solution transfer and precipitation and high deformability of K-feldspar by dislocation creep may have maintained this high ductility of the bands. What condition brought the high ductility remains to be solved.

8. Conclusion

1. The microstructural changes from mylonites to banded ultramylonites in studied mylonites, deformed under an upper greenschist facies condition, include a decrease in modal proportion and grain size of plagioclase and K-feldspar porphyroclasts, a development of Pl > Kfs (>Qtz + Bt) bands and Kfs bands and an increase in modal content of Pl > Kfs (>Qtz + Bt) bands. The dominant processes for grain size reduction of porphyroclasts were the fracturing of plagioclase and the replacement of K-feldspar by myrmekite. The aqueous K^+ formed by the replacement precipitated as K-feldspar, in fractures and tails on porphyroclasts, to form Pl > Kfs (>Qtz + Bt) bands and Kfs bands. K-feldspar in the Kfs bands was further replaced by myrmekite and myrmekite itself changed to Pl > Kfs (>Qtz + Bt) bands with increasing strain. In this way, the modal proportion of porphyroclasts decreased and that of Pl > Kfs (>Qtz + Bt) bands increased with increasing mylonitization.
2. Qtz bands were deformed by dislocation creep with the dominant slip system of prism <*a*>, accompanied by rotation recrystallization. Pl > Kfs (>Qtz + Bt) bands were developed through fracturing of plagioclase porphyroclasts and filling the space by K-feldspar. Kfs bands may be formed by precipitation from solution, and then deformed by dislocation creep indicated by the development of CPO. Kfs > Pl > Qtz bands were developed through dislocation creep of Kfs bands and simultaneous formation of myrmekite along grain boundaries of K-feldspar.
3. The development of the banded structure was promoted by high mobility of K-feldspar through myrmekite replacement, solution transfer and precipitation.
4. Because both Pl > Kfs (>Qtz + Bt) bands and Kfs > Pl > Qtz bands show clear spatial distribution of

constituent minerals, instead of homogeneous mixing of them, the grain boundary sliding was not the dominant deformation process.

Acknowledgements

We would like to thank J. Tullis and J. Wheeler for thorough and constructive reviews and T. G. Blenkinsop for editorial handling. This study was supported by Grant 13304042 and 17340159 from the Ministry of Education, Science and Culture of Japan to K. Kanagawa.

References

Banno, S., Nakajima, T., 1992. Metamorphic belts of Japanese Islands. Annual Review of Earth and Planetary Sciences 20, 159–179.

Behrmann, J.H., Mainprice, D., 1987. Deformation mechanisms in a high-temperature quartz-feldspar mylonite: evidence for superplastic flow in the lower continental crust. Tectonophysics 140, 297–305.

Blumenfeld, P., Mainprice, D., Bouchez, J.-L., 1986. C-slip in quartz from subsolidus deformed granite. Tectonophysics 127, 97–115.

Bouchez, J.L., 1977. Plastic deformation of quartzites at low temperature in an area of natural strain gradient. Tectonophysics 39, 25–50.

Brown, B.E., Bailey, S.W., 1964. The structure of maximum microcline. Acta Crystallographica 17, 1391–1400.

Fliervoet, T.F., White, S.H., Drury, M.R., 1997. Evidence for dominant grain-boundary sliding deformation in greenschist- and amphibolite-grade polymineralic ultramylonites from the Redbank Deformed Zone, Central Australia. Journal of Structural Geology 19, 1495–1520.

Guillope, M., Poirier, J.P., 1979. Dynamic recrystallization during creep of single-crystalline halite: an experimental study. Journal of Geophysical Research 84, 5557–5567.

Handy, M.R., 1990. The solid state flow of polymineralic rocks. Journal of Geophysical Research 95, 8647–8661.

Heilbonner, R., Tullis, J., 2002. The effect of static annealing on microstructures and crystallographic preferred orientations of quartzites experimentally deformed in axial compression and shear. In: De Meer, S., Drury, M.R., De Bresser, J.H.P., Pennock, G.M. (Eds.), Deformation Mechanisms, Rheology and Tectonics: Current Status and Future Perspectives. Geological Society, London, Special Publications, vol. 200, pp. 191–218.

Hippertt, J.F., 1998. Breakdown of feldspar, volume gain and lateral mass transfer during mylonitization of granitoid in a low metamorphic grade shear zone. Journal of Structural Geology 20, 175–193.

Hirth, G., Tullis, J., 1992. Dislocation creep regimes in quartz aggregates. Journal of Structural Geology 14, 145–160.

Imon, R., Okudaira, T., Fujimoto, A., 2002. Dissolution and precipitation processes in deformed amphibolites: an example from the ductile shear zone of the Ryoke metamorphic belt, SW Japan. Journal of Metamorphic Geology 20, 297–308.

Imon, R., Okudaira, T., Kanagawa, K., 2004. Development of shape- and lattice-preferred orientations of amphibole grains during initial cataclastic deformation and subsequent deformation by dissolution–precipitation creep in amphibolites from the Ryoke metamorphic belt, SW Japan. Journal of Structural Geology 26, 793–805.

Itihara, M., Ichikawa, K., Yamada, N., 1986. Geology of the Kishiwada District. Quadrangle series, Scale 1:50,000. Geological Survey of Japan, Tsukuba (in Japanese with English abstract).

Lister, G.S., Dornsiepen, U.F., 1982. Fabric transitions in the Saxony granulite terrain. Journal of Structural Geology 4, 81–92.

Lloyd, G.E., 1987. Atomic number and crystallographic contrast images with the SEM: a review of backscattered techniques. Mineralogical Magazine 51, 3–19.

Lloyd, G.E., Farmer, A.B., Mainprice, D., 1997. Misorientation analysis and the formation and orientation of subgrain and grain boundaries. Tectonophysics 279, 55–78.

Mainprice, D., Bouchez, J.-L., Blumenfeld, P., Tubiá, J.M., 1986. Dominant c slip in naturally deformed quartz: implications for dramatic plastic softening at high temperature. Geology 14, 819–822.

Mancktelow, N.S., 1987. Atypical textures in quartz veins from Simplon Fault Zone. Journal of Structural Geology 9, 995–1005.

Marshall, D.J., 1988. Cathodoluminescence of Geological Materials. Unwin Hyman, Boston.

Menegon, L., Pennacchioni, G., Stünitz, H., 2006. Nucleation and growth of myrmekite during ductile shear deformation in metagranites. Journal of Metamorphic Geology 24, 553–568.

Neumann, B., 2000. Texture development of recrystallized quartz polycrystals unravelled by orientation and misorientation characteristics. Journal of Structural Geology 22, 1695–1711.

Okudaira, T., Takeshita, T., Hara, I., Ando, J., 1995. A new estimate of the conditions for transition from basal $<a>$ to prism $[c]$ slip in naturally deformed quartz. Tectonophysics 250, 31–46.

Poirier, J.P., Nicolas, A., 1975. Deformation-induced recrystallization by progressive misorientation of subgrain-boundaries, with special reference to mantle peridotites. Journal of Geology 83, 707–720.

Prior, D.J., Trimby, P.W., Weber, U.D., Dingley, D.J., 1996. Orientation contrast imaging of microstructures in rocks using forescatter detectors in the scanning electron microscope. Mineralogical Magazine 60, 859–869.

Ree, J.-H., Kim, H.S., Han, R., Jung, H., 2005. Grain-size reduction of feldspars by fracturing and neocrystallization in a low-grade granitic mylonite and its rheological effect. Tectonophysics 407, 227–237.

Randle, V., 2003. Microtexure Determination and Its Applications, second ed. Maney Publishing, London.

Sakakibara, N., 1995. Structural evolution of multiple ductile shear zone system in the Ryoke belt, Kinki Province. Journal of Science of the Hiroshima University Series C (Geology and Mineralogy) 10, 267–332.

Schmid, S.M., Casey, M., 1986. Complete fabric analysis of some commonly observed quartz *c*-axis patterns. In: Hobbs, B.E., Heard, H.C. (Eds.), Mineral and Rock Deformation Laboratory Studies: The Paterson Volume. American Geophysical Union, Geophysical Monograph, vol. 36, pp. 263–286.

Schulmann, K., Mlcoch, B., Melka, R., 1996. High-temperature microstructures and rheology of deformed granite, Erzgebirge, Bohemian Massif. Journal of Structural Geology 18, 719–733.

Shigematsu, N., Yamagishi, H., 2002. Quartz microstructures and deformation conditions in the Hatagawa shear zone, north-eastern Japan. Island Arc 11, 45–60.

Simpson, C., Wintch, R.P., 1989. Evidence for deformation-induced K-feldspar replacement by myrmekite. Journal of Metamorphic Geology 7, 261–275.

Stipp, M., Stunitz, H., Heilbronner, R., Schmid, S.M., 2002. The eastern Tonale fault zone: a 'natural laboratory' for crystal plastic deformation of quartz over a temperature range from 250 °C to 700 °C. Journal of Structural Geology 24, 1861–1884.

Stipp, M., Tullis, J., Behrens, H., 2006. Effect of water on the dislocation creep microstructure and flow stress of quartz and implications for the recrystallized grain size piezometer. Journal of Geophysical Research 111, B04201, doi:10.1029/2005JB003852.

Stünitz, H., Fitz Gerald, J.D., 1993. Deformation of granitoids at low metamorphic grade. II: granular flow in albite-rich mylonites. Tectonophysics 221, 299–324.

Suzuki, K., Adachi, M., 1998. Denudation history of the high T/P Ryoke metamorphic belt, southwest Japan: constraints from CHIME monazite ages of gneisses and granitoids. Journal of Metamorphic Geology 16, 23–38.

Tagami, M., Takeshita, T., 1998. *c*-Axis fabrics and microstructures in quartz schist from the Sambagawa metamorphic belt, central Shikoku, Japan. Journal of Structural Geology 20, 1549–1568.

Takagi, H., 1986. Implications of mylonitic microstructures for the geotectonic evolution of the Median Tectonic Line, central Japan. Journal of Structural Geology 8, 3–14.

Takagi, H., Mizutani, T., Hirooka, K., 1988. Deformation of quartz in an inner shear zone of the Ryoke belt – an example in the Kishiwada area, Osaka Prefecture. Journal of the Geological Society of Japan 94, 869–886 (in Japanese with English abstract).

Takeshita, T., Wenk, H.-R., 1988. Plastic anisotropy and geometrical hardening in quartzites. Tectonophysics 149, 345–361.

Tsurumi, J., Hosonuma, H., Kanagawa, K., 2003. Strain localization due to a positive feedback of deformation and myrmekite-forming reaction in granite and aplite mylonites along the Hatagawa Shear Zone of NE Japan. Journal of Structural Geology 25, 557–574.

Tullis, J., 1983. Deformation of feldspars. In: Ribbe, P.H. (Ed.), Feldspar Mineralogy. Reviews in Mineralogy, vol. 2. Mineralogical Society of America, pp. 297–323.

Wheeler, J., Jiang, Z., Prior, D.J., Tullis, J., Drury, M.R., Trimby, P.W., 2003. From geometry to dynamics of microstructure: using boundary lengths to quantify boundary misorientations and anisotropy. Tectonophysics 376, 19–35.

Wheeler, J., Prior, D.J., Jiang, Z., Spiess, R., Trimby, P.W., 2001. The petrological significance of misorientations between grains. Contributions to Mineralogy and Petrology 141, 109–124.

White, S., 1977. Geological significance of recovery and recrystallization processes in quartz. Tectonophysics 39, 143–170.

Wilson, C.J.L., 1975. Preferred orientation in quartz ribbon mylonites. Geological Society of America Bulletin 86, 968–974.

Yagi, K., Takeshita, T., 2002. Regional variation in exhumation and strain rate of the high-pressure Sambagawa metamorphic rocks in central Shikoku, south-west Japan. Journal of Metamorphic Geology 20, 633–647.